

GODDARD
GRANT

IN-19-CR

69281

p. 17



SCHOOL OF ENGINEERING
& ARCHITECTURE



The Catholic University of America
Washington, DC 20064

(NASA-CR-189861) ANALYSIS AND EXPERIMENTAL EVALUATION OF A STEWART PLATFORM-BASED FORCE/TORQUE SENSOR Semiannual Progress Report, 1 Jul. 1991 - 1 Feb. 1992 (Catholic Univ. of America) 17 p N92-17150 Unclass CSCL 22B 63/19 0069281

**THE CATHOLIC UNIVERSITY OF AMERICA
DEPARTMENT OF ELECTRICAL ENGINEERING**

Semiannual Progress Report

**ANALYSIS AND EXPERIMENTAL
EVALUATION OF
A STEWART PLATFORM-BASED
FORCE/TORQUE SENSOR**

Grant Number NAG 5-780

Charles C. Nguyen
Principal Investigator and Associate Professor
and
Sami S. Antrazi
Graduate Research Assistant

submitted to
Dr. Charles E. Campbell, Jr.
Code 714.1
Goddard Space Flight Center (NASA)
Greenbelt, Maryland

January 1992

Contents

1	Introduction	2
2	The Force/Torque Sensor System	3
2.1	The Force/Torque Sensor	3
2.2	The Data Acquisition System	3
3	Force Sensor Inverse Kinematics	4
4	Force Sensor Forward Kinematics	6
5	Computation of Forces/Torques	7
6	Experimental Verification	8
7	Conclusion	9

SUMMARY

This report deals with the kinematic analysis and experimentation of a force/torque sensor whose design is based on the mechanism of the Stewart Platform. Besides being used for measurement of forces/torques, the sensor also serves as a compliant platform which provides passive compliance during a robotic assembly task. It consists of two platforms, the upper compliant platform (UCP) and the lower compliant platform (LCP), coupled together through six spring-loaded pistons whose length variations are measured by six linear voltage differential transformers (LVDT) mounted along the pistons. Solutions to the forward and inverse kinematics of the force sensor are derived. Based on the known spring constant and the piston length changes, forces/torques applied to the LCP gripper are computed using vector algebra. Results of experiments conducted to evaluate the sensing capability of the force sensor are reported and discussed.

1 Introduction

For high precision tasks where the requirements of accuracy and sturdiness outweigh these of large workspace and maneuverability, closed-kinematic chain (CKC) mechanisms are more often employed than the conventional anthropomorphic open-kinematic chain (OKC) mechanism to design robotic manipulators, end-effectors and devices performing the tasks [1]-[27]. This comes from the fact that CKC robots are generally sturdier and more precise than OKC robots because of the closed chain nature of their mechanisms. Having links and joints actuating in series and being compact, OKC robots possess long reach, large workspace and are capable of entering small spaces. However the cantilever-like structure causes them to have low stiffness and undesired dynamic characteristics, especially at high speed and large payload. Moreover, due to the nonuniform distribution of payload to actuators and serial accumulation of joint errors throughout the OKC mechanism, OKC robots have low strength-to-weight ratios and are not capable of providing high precision motion needed in robotic assembly tasks. On the other hand, CKC robots whose mechanism are parallel, have been considered in numerous robotic applications because of their high structural rigidity and non-serial accumulation of joint and link errors. One of the first applications of CKC mechanism appeared in the design of the Stewart Platform [1] which was later employed by Dieudonne and his coworkers [2] to design an aircraft simulator at the NASA Langley Research Center. Hoffman and McKinnon [3] used a finite element program to simulate the motion of the Stewart Platform whose mechanism was later applied by McCallion and Truong [4] to design an automatic table. Hunt [5,7] studied the structural kinematic problem of in-parallel-actuated robot manipulators. Applying linear algebra elements to screw systems, Sugimoto and Duffy [6] developed a general method to describe the instantaneous link motion of a single closed-loop mechanism. In order to investigate autonomous part assembly in space, Premack and others [8] of NASA/Goddard Space Flight Center designed and built a passive compliant robot end-effector whose active compliance problem was later investigated by Nguyen and his coworkers [9]. The kinematic problems and practical construction of the Stewart Platform were considered by Yang and Lee [10], Mohammed and Duffy [11], and Fichter [12]. Sugimoto [13] studied kinematics and dynamics of parallel manipulators and Lee and his coworkers [14] derived dynamical equations for a 3 degree-of-freedom (DOF) manipulator. Rees-Jones [15] applied screw theory to treat Stewart Platform-based manipulators while Sharon and others [17] applied the Stewart Platform mechanism to design a micromanipulator performing

fine motion. The Stewart Platform mechanism was also applied by Kerr [19] to manufacture a force/torque sensor. Other problems of Stewart Platform-based manipulators such as adaptive force/torque control, kinematics, dynamics and workspace computation were treated by Nguyen and his coworkers [20,22,23]. Closed-form solutions of forward kinematics were derived by Griffis and Duffy [21] and Nanua and others [24] for a class of Stewart Platforms. Nguyen and others [25,26] developed learning control and trajectory planning schemes for parallel manipulators and presented experimental results of the trajectory planning schemes in [27].

This report deals with the kinematic analysis and experimentation of a six-degree-of-freedom force/torque sensor whose design is based on the mechanism of the Stewart Platform. The paper is organized as follows. Section 2 describes and explains the functions of the main components of the force/torque sensor system. Sections 3 and 4 present the solutions to inverse and forward kinematics of the force/torque sensor, respectively. Vector equations are developed in Section 5 for computing forces/torques. Section 6 presents results of experiments conducted to evaluate the sensing capability of the force sensor. Finally the content of the paper will be reviewed and future research activities will be outlined in Section 7.

2 The Force/Torque Sensor System

Figure 1 presents the force/torque system which mainly consists of a 6 DOF force/torque sensor, a data acquisition system and an AT 286 personal computer. The main components and the functions of the force/torque sensor and the data acquisition system are described below.

2.1 The Force/Torque Sensor

Figure 2 shows the force sensor¹ which is composed of an upper compliant platform (UCP) and a lower compliant platform (LCP) coupled together through six spring-loaded pistons arranged in a geometry similar to the mechanism of the Stewart Platform. Universal joints are used to mount the pistons to the two platforms. A gripper is attached to the LCP to perform assembly of parts. The pistons permit strain on two opposing springs acting in each piston. They are compressed or extended when resistive or gravitational forces are exerted on the gripper. Thus the force sensor mechanism also serves as a passive compliant device which provides compliance to the gripper during an assembly task. TRANS-TEK DC-DC gaging linear voltage differential transformers (LVDT) are mounted along the pistons to measure the deflection of the springs, which will be used to calculate forces/torques applied to gripper. The supply voltage is provided by a KEPCE ATE 15-3P power supply, a very stable variable voltage power supply which is especially suitable for high precision measurement.

2.2 The Data Acquisition System

As presented in Figure 1, LVDT analog signals representing the corresponding spring deflections are processed through a CAMAC data acquisition system which consists of an Analog-to-Digital Converter (ADC) board, a Display Controller board, a Dataway display board, a CRATE controller board, and a Personal Computer (PC) interface board, all contained in a CAMAC Crate. The CAMAC Crate acts as a house for up to 25 boards and several busways

¹For simplicity, from now on, *force sensor* is used to denote *force/torque sensor*.

for board communication, and provides DC power to the boards. The ADC board can convert up to 16 analog voltages into equivalent digital values using a sample-and-hold amplifier and a successive-approximation converter. The LVDT signals are continuously scanned and converted, and the results are then stored in the module's 16-word memory. The Dataway Display module indicates the state of all the Dataway signal lines during a Dataway cycle. It contains two 24-bit registers, designated as Data and Command register whose outputs are continuously displayed by front-panel LEDs. The Crate Controller provides an asynchronous, parallel data path between a CAMAC crate and a parallel I/O port of a computer. A 50-contact, flat-ribbon connector is used for the reception and transmission of all necessary data and control lines between the Crate Controller and the interface device which are 16 bits wide. The Crate Controller is accessed by calling assembly language routines which indicate to the system the type of information requested.

3 Force Sensor Inverse Kinematics

This section presents the development of kinematic equations which can be used to convert the piston lengths measured by the LVDTs into the corresponding pose² of the LCP with respect to the UCP. Figure 3 shows two right-hand coordinate frames $\{\mathbf{A}\}$ and $\{\mathbf{E}\}$ assigned to the UCP and LCP, respectively. The Centroid A of the UCP is chosen to be the origin of Frame $\{\mathbf{A}\}$, the \mathbf{z}_A -axis is pointing outward and the \mathbf{x}_A -axis is perpendicular to the line connecting the two attachment points A_1 and A_6 . In addition, θ_A denotes the angle between A_1 and A_2 . The angles between A_1 and A_3 and between A_3 and A_5 are set to 120° to obtain a symmetrical distribution of joints on the UCP. Similarly, the Centroid E of the LCP is the origin of Frame $\{\mathbf{E}\}$, the \mathbf{x}_E -axis is perpendicular to the line connecting the two attachment points E_1 and E_6 , and θ_E denotes the angle between E_1 and E_2 . Also the angles between E_1 and E_3 and between E_3 and E_5 are set to 120° in order to symmetrically distribute the joints on the LCP. The Cartesian variables are chosen to be the relative pose of Frame $\{\mathbf{E}\}$ with respect to Frame $\{\mathbf{A}\}$ where the position of Frame $\{\mathbf{E}\}$ is specified by the position of its origin with respect to Frame $\{\mathbf{A}\}$. Now if we denote the angle between AA_i and \mathbf{x}_A by λ_i , and the angle between EE_i and \mathbf{x}_E by Λ_i for $i=1,2,\dots,6$, then

$$\Lambda_i = 60i^\circ - \frac{\theta_E}{2}; \lambda_i = 60i^\circ - \frac{\theta_A}{2}, \text{ for } i = 1, 3, 5 \quad (1)$$

and

$$\Lambda_i = \Lambda_{i-1} + \theta_E; \lambda_i = \lambda_{i-1} + \theta_A, \text{ for } i = 2, 4, 6. \quad (2)$$

Furthermore, if Vector ${}^E\mathbf{e}_i = (e_{ix} \ e_{iy} \ e_{iz})^T$ describes the position of the attachment point E_i with respect to Frame $\{\mathbf{E}\}$, and Vector ${}^A\mathbf{a}_i = (a_{ix} \ a_{iy} \ a_{iz})^T$ the position of the attachment point A_i with respect to Frame $\{\mathbf{A}\}$, then they can be written as

$${}^E\mathbf{e}_i = \begin{bmatrix} r_E \cos(\lambda_i) & r_E \sin(\lambda_i) & 0 \end{bmatrix}^T \quad (3)$$

and

$${}^A\mathbf{a}_i = \begin{bmatrix} r_A \cos(\Lambda_i) & r_A \sin(\Lambda_i) & 0 \end{bmatrix}^T \quad (4)$$

for $i=1,2,\dots,6$ where r_A and r_E represent the radii of the UCP and LCP, respectively.

²In this report, *pose* implies both *position and orientation*.

Let us now consider the vector diagram for an i th piston given in Figure 4. The position of Frame $\{\mathbf{E}\}$ is represented by Vector ${}^A\mathbf{d} = [x \ y \ z]^T$ which contains the Cartesian coordinates x , y , z of the origin of Frame $\{\mathbf{E}\}$ with respect to Frame $\{\mathbf{A}\}$. The length vector ${}^A\mathbf{q}_i = (q_{ix} \ q_{iy} \ q_{iz})^T$, expressed with respect to Frame $\{\mathbf{A}\}$ can be computed by

$${}^A\mathbf{q}_i = {}^A\mathbf{x}_i + {}^A\mathbf{e}_i \quad (5)$$

where

$${}^A\mathbf{x}_i = {}^A\mathbf{d} - {}^A\mathbf{a}_i \quad (6)$$

$$= \begin{bmatrix} x - a_{ix} \\ y - a_{iy} \\ z - a_{iz} \end{bmatrix} = \begin{bmatrix} x - a_{ix} \\ y - a_{iy} \\ z \end{bmatrix} = \begin{bmatrix} \bar{x}_i \\ \bar{y}_i \\ \bar{z}_i \end{bmatrix} \quad (7)$$

which is a shifted vector of ${}^A\mathbf{d}$ and

$${}^A\mathbf{e}_i = {}^A\mathbf{R} \ {}^E\mathbf{e}_i \quad (8)$$

$$= \begin{bmatrix} r_{11} & r_{12} & r_{13} \\ r_{21} & r_{22} & r_{23} \\ r_{31} & r_{32} & r_{33} \end{bmatrix} \begin{bmatrix} e_{ix} \\ e_{iy} \\ e_{iz} \end{bmatrix} = \begin{bmatrix} r_{11}e_{ix} + r_{12}e_{iy} \\ r_{21}e_{ix} + r_{22}e_{iy} \\ r_{31}e_{ix} + r_{32}e_{iy} \end{bmatrix} = \begin{bmatrix} u_i \\ v_i \\ w_i \end{bmatrix} \quad (9)$$

which is the representation of ${}^A\mathbf{e}_i$ in Frame $\{\mathbf{A}\}$ and ${}^A\mathbf{R}$ is the *Orientation Matrix* representing the orientation of Frame $\{\mathbf{E}\}$ with respect to Frame $\{\mathbf{A}\}$.

Thus the length l_i of Vector ${}^A\mathbf{q}_i$ can be computed from its components as

$$l_i = \sqrt{q_{ix}^2 + q_{iy}^2 + q_{iz}^2}. \quad (10)$$

or

$$l_i = \sqrt{(\bar{x}_i + u_i)^2 + (\bar{y}_i + v_i)^2 + (\bar{z}_i + w_i)^2} \quad (11)$$

We obtain from (3)-(4)

$$e_{ix}^2 + e_{iy}^2 + e_{iz}^2 = r_E^2, \quad (12)$$

$$a_{ix}^2 + a_{iy}^2 + a_{iz}^2 = r_A^2. \quad (13)$$

and from the properties of orientation matrix

$$r_{11}^2 + r_{21}^2 + r_{31}^2 = r_{12}^2 + r_{22}^2 + r_{32}^2 = r_{13}^2 + r_{23}^2 + r_{33}^2 = 1 \quad (14)$$

and

$$\begin{aligned} r_{11}r_{12} + r_{21}r_{22} + r_{31}r_{32} &= 0 \\ r_{11}r_{13} + r_{21}r_{23} + r_{31}r_{33} &= 0 \\ r_{12}r_{13} + r_{22}r_{23} + r_{32}r_{33} &= 0. \end{aligned} \quad (15)$$

Using (12)-(15), Equation (10) can be rewritten as

$$\begin{aligned} l_i^2 &= x^2 + y^2 + z^2 + r_E^2 + r_A^2 + 2(r_{11}e_{ix} + r_{12}e_{iy})(x - a_{ix}) \\ &\quad + 2(r_{21}e_{ix} + r_{22}e_{iy})(y - a_{iy}) + 2(r_{31}e_{ix} + r_{32}e_{iy})z \\ &\quad - 2(xa_{ix} + ya_{iy}), \end{aligned} \quad (16)$$

for $i=1,2,\dots,6$.

Equation (16) represents the *closed-form* solution to the force sensor inverse kinematics in the sense that piston lengths l_i for $i=1,2,\dots,6$ which correspond to the pose of Frame $\{\mathbf{E}\}$ with respect to Frame $\{\mathbf{A}\}$ can be determined using (16).

The orientation of Frame $\{\mathbf{E}\}$ with respect to Frame $\{\mathbf{A}\}$ can be described by the orientation matrix ${}^{\mathbf{A}}\mathbf{R}$ as shown in (9) which requires nine variables r_{ij} for $i,j=1,2,3$ from which six are redundant because only three are needed to specify an orientation [30]. There exist several ways to specify an orientation by three variables, but the most widely used one is the Roll-Pitch-Yaw angles α , β , and γ , which represent the orientation of Frame $\{\mathbf{E}\}$, obtained after the following sequence of rotations from Frame $\{\mathbf{A}\}$:

1. First rotate Frame $\{\mathbf{A}\}$ about the x_A -axis an angle γ (*Yaw*),
2. Then rotate the resulting frame about the y_A -axis an angle β (*Pitch*), and
3. Finally rotate the resulting frame about the z_A -axis an angle α (*Roll*).

The orientation represented by the above Roll-Pitch-Yaw angles is given by³

$${}^{\mathbf{A}}\mathbf{R} = \mathbf{R}_{RPY} = \begin{bmatrix} c\alpha c\beta & c\alpha s\beta s\gamma - s\alpha c\gamma & c\alpha s\beta c\gamma + s\alpha s\gamma \\ s\alpha c\beta & s\alpha s\beta s\gamma + c\alpha c\gamma & s\alpha s\beta c\gamma - c\alpha s\gamma \\ -s\beta & c\beta s\gamma & c\beta c\gamma \end{bmatrix}. \quad (17)$$

4 Force Sensor Forward Kinematics

This section deals with the conversion of the lengths l_i for $i=1,2,\dots,6$ measured by six LVDTs into the pose of Frame $\{\mathbf{E}\}$ with respect to Frame $\{\mathbf{A}\}$. This type of conversion is the force sensor forward kinematics which can be formulated as to find a Cartesian position specified by x , y , z and an orientation specified by Roll-Pitch-Yaw angles α , β , and γ to satisfy Equation (16) for a given set of pistons lengths l_i for $i=1,2,\dots,6$. In general, there exists no closed-form solution for the above problem since Equation (16) represents a set of 6 highly nonlinear simultaneous equations with 6 unknowns. Consequently iterative numerical methods must be employed to solve the above set of nonlinear equations. In the following we will present the implementation of Newton-Raphson method for solving the forward kinematic problem.

In order to apply the Newton-Raphson method, first from (11) we define 6 scalar functions

$$f_i(\boldsymbol{\sigma}) = (\bar{x}_i + u_i)^2 + (\bar{y}_i + v_i)^2 + (\bar{z}_i + w_i)^2 - l_i^2 = 0 \quad (18)$$

for $i=1,2,\dots,6$, where the vector $\boldsymbol{\sigma}$ is defined as

$$\boldsymbol{\sigma} = \left[\sigma_1 \quad \sigma_2 \quad \sigma_3 \quad \sigma_4 \quad \sigma_5 \quad \sigma_6 \right]^T = \left[x \quad y \quad z \quad \alpha \quad \beta \quad \gamma \right]^T, \quad (19)$$

and then employ the following algorithm [29] to solve for $\boldsymbol{\sigma}$:

Algorithm 1: Force Sensor Forward Kinematics

³ $c\alpha \equiv \cos \alpha$, and $s\alpha \equiv \sin \alpha$.

Step 1: Select an initial guess σ .

Step 2: Compute the elements r_{ij} of ${}^A_E\mathbf{R}$ using (17) for $i,j=1,2,3$.

Step 3: Compute $\bar{x}_i, \bar{y}_i, \bar{z}_i$, using (7) and u_i, v_i, w_i using (9) for $i=1,2,\dots,6$.

Step 4: Compute $f_i(\sigma)$ and $A_{ij} = \frac{\partial f_i}{\partial \sigma_j}$ using (18) for $i, j=1,2,\dots,6$.

Step 5: Compute $B_i = -f_i(\sigma)$ for $i=1,2,\dots,6$. If $\sum_{j=1}^6 |B_j| < \text{tol}$ (tolerance), stop and adopt σ as the solution.

Step 6: Solve $\sum_{j=1}^6 A_{ij} \delta\sigma_j = B_i$ for $\delta\sigma_j$ for $i,j=1,2,\dots,6$ using LU decomposition. If $\sum_{j=1}^6 \delta\sigma_j < \text{tol}$ (tolerance), stop and adopt σ as the solution.

Step 7: Select $\sigma^{\text{new}} = \sigma + \delta\sigma$ and repeat Steps 1-7.

5 Computation of Forces/Torques

In this section, we will derive mathematical expressions which utilize the spring deflections measured by the LVDTs to compute the forces applied to the gripper. The forces will be computed with respect to Frame $\{\mathbf{A}\}$ of the UCP. When external forces are applied to the gripper, the gripper will deflect. An equilibrium is achieved when the forces created in the 6 pistons and its corresponding torques balance out the external force and torques, respectively [28]. In general, an external force applied to the gripper creates forces in the pistons and no torque about the gripper position G. An external torque which results from a pair of forces equal in magnitude, opposite in direction, and on parallel lines of action will create piston forces that cancel out each other and the resultant torque of all the torques created by the piston forces is equal to the external torque.

We proceed to consider the vector diagram in Figure 4 which represents the LCP relative to the UCP after a set of external forces and torques are applied to a point G on the gripper. The current piston lengths, $l_{i,\text{new}}$ for $i=1,2,\dots,6$ can be computed by

$$l_{i,\text{new}} = l_{i,\text{old}} + \Delta l_i \quad (20)$$

where $l_{i,\text{old}}$ for $i=1,2,\dots,6$ are the piston lengths before the external forces and torques are applied and Δl_i for $i=1,2,\dots,6$ are the changes in piston lengths, measured and provided by the LVDTs. A force vector is expressed as the product of its magnitude and the unit vector of the position vector along which the force is acting [28]. The position vector ${}^A\mathbf{q}_i$ along which the force acts on the piston is computed by

$${}^A\mathbf{q}_i = {}^A\mathbf{d} - {}^A\mathbf{a}_i + {}^A_E\mathbf{R} {}^E\mathbf{e}_i \quad (21)$$

where ${}^A\mathbf{d}$ and ${}^A_E\mathbf{R}$ which represent the current position and orientation of Frame $\{\mathbf{E}\}$ with respect to Frame $\{\mathbf{A}\}$, respectively, are computed by applying Algorithm 1 on $l_{i,\text{new}}$. Thus the force acting on the i th piston is obtained by

$$\mathbf{F}_i = K_i \Delta l_i \frac{{}^A\mathbf{q}_i}{|{}^A\mathbf{q}_i|} \quad (22)$$

where K_i denotes the equivalent spring constant of the two springs acting in the piston and ${}^A\mathbf{q}_i/|{}^A\mathbf{q}_i|$ denotes the unit vector of the position vector along which \mathbf{F}_i acts and $|{}^A\mathbf{q}_i|$ denotes the magnitude of the position vector. Furthermore, the extension, or compression, of the springs Δl_i is positive when \mathbf{F}_i is tensile and negative when \mathbf{F}_i is compressive. In other words, the force which the springs of the i th piston applies on the gripper is equal to $-\mathbf{F}_i$.

Thus when the gripper location G is in equilibrium, the force applied to the gripper is equal to the resultant force of the piston forces, namely

$$\mathbf{F} = \sum_{i=1}^6 \mathbf{F}_i = \sum_{i=1}^6 K_i \Delta l_i \frac{{}^A\mathbf{q}_i}{|{}^A\mathbf{q}_i|}. \quad (23)$$

As discussed above, from the fact that the torque about G caused by the external force applied at G is equal to zero, the external torque, \mathbf{M} about G is equal to the resultant torque about G caused by the piston forces when the gripper is in equilibrium. Thus

$$\mathbf{M} = \sum_{i=1}^6 {}^A\mathbf{h}_i \times \mathbf{F}_i = \sum_{i=1}^6 {}^A\mathbf{h}_i \times K_i \Delta l_i \frac{{}^A\mathbf{q}_i}{|{}^A\mathbf{q}_i|} \quad (24)$$

where

$${}^A\mathbf{h}_i = {}^A\mathbf{d} - {}^A\mathbf{a}_i + \frac{{}^A\mathbf{R}}{E} {}^E\mathbf{g}_i, \quad (25)$$

and \times denotes the vector product.

6 Experimental Verification

In this section, experiments are performed to evaluate the sensing capability of the force sensor. In the following two experiments, the data of the piston lengths provided by the LVDTs are acquired *on-line* via the data acquisition system and stored on the hard disk of the personal computer. After each experiment, computation of forces and torques are carried out *off-line* using a program written in C language, which implements the force sensor inverse and forward kinematics and the force computations. Then MATLAB is used to graphically display the obtained results.

Experiment 1: Measurement of Pure Torques

The first experiment is designed to test the force sensor capability of measuring pure torques. First the force sensor as shown in Figure 2 is calibrated to compensate any gravitational forces caused by the masses of the gripper assembly and the stepper motor driving the gripper mechanism. This is done by setting the LVDT signals all to zero when the force sensor mechanism is in a *symmetrical* and *unloaded* pose by ensuring that the lengths l_i for $i=1,2,\dots,6$ as expressed in Equation (10) are exactly equal to each other. Weights can be externally added to the gripper mechanism to achieve the symmetrical and unloaded pose. In addition, before the experiment, the force sensor is calibrated by applying some known vertical force to the gripper using a force gauge and setting and scaling the LVDT signals accordingly.

In order to apply a positive (negative) torque to the gripper, we rotate the gripper about an axis \mathbf{z}_G which emanates from G and is parallel to \mathbf{z}_E , as shown in Figure 4 an angle of 2

degrees (-2 degrees) while keeping the force sensor UCP at a fixed pose. Since only torque is applied to the gripper, it is expected that only torque and no force is sensed by the force sensor. Indeed, according to the experimental results, the forces acquired in the directions of x_A -axis, y_A -axis, and z_A -axis are very negligible, which may be created by imperfect calibration of the LVDTs. Figure 5 presents the time history of the force signals. As expected, the torques about G assumes a value of 2.303 lb-in and -2.1919 lb-in when the gripper is rotated an angle of 2 degrees and -2 degrees, respectively.

Experiment 2: Force Measurement During Connector Mating

In the second experiment, we use the force sensor to monitor the forces applied to the gripper during the mating and demating of a space-rated connector, Series 882, manufactured by G & H Technology, Inc.

The UCP of the force sensor is mounted to the payload platform of a Stewart Platform-based robot manipulator [27] whose linear actuators are driven by stepper motors. The gripper motion during the connector mating/demating is created by properly controlling the motion of the stepper motors. The forces applied along the x_A -axis, y_A -axis and z_A -axis are reported in Figures 6, 7, and 8, respectively. The mating and demating are performed in two different stages. In the first stage, the connector is mated and demated under a perfect alignment between the connector plug and the connector receptacle and in the second stage under a misalignment produced by rotating the connector plug about the z_G -axis an angle of -2 degrees. The force applied in the z_A -axis is the largest as compared to those applied in the x_A -axis and y_A -axis since the gripper motion during the mating and demating is mostly vertical. As shown in Figure 8, the forces exerted along the z_A -axis during the demating in both stages are of almost the same value of about 26.23 lb. Figure 8 also shows that the maximum forces required for the mating are 28.024 lb and 39.84 lb during the first and second stage, respectively and the force is relatively disturbed during the second stage because of the misalignment. Figure 6 and 7 show that the forces applied along x_A -axis and y_A -axis do not exceed 2 lbs because the mating and demating are performed vertically as mentioned above. The mating and demating of the same connector is then repeated under various misalignments. Figure 9 plots the maximum and average mating forces versus the misalignment degrees. As expected, the mating forces are positively proportional to the misalignment degrees as shown in the figure.

7 Conclusion

In this report, we have presented the development of the inverse and forward kinematics of a 6 DOF Stewart Platform-based force sensor which is mainly composed of two platforms coupled together by 6 spring-loaded pistons. The force sensor mechanism is also used as a passive compliance device which provides compliance during part assembly tasks. The forces and torques applied to a gripper mounted to the lower compliant platform of the force sensor were computed using the force sensor inverse and forward kinematic equations, the equivalent spring constants and the piston length variations measured by LVDTs mounted along the pistons. Experiments conducted to evaluate the sensing capability of the force sensor showed that it is capable of measuring torque applied to the gripper and of monitoring transient forces applied during the mating and demating of a space-rated connector. The force sensor kinematic equations have

been optimized and are currently fast enough for real-time force computation. We will shortly report results of experiments such as mating/demating connectors and replacement of orbital replaceable units, which are performed under force feedback.

References

- [1] Stewart, D., "A Platform with Six Degrees of Freedom," *Proc. Institute of Mechanical Engineering*, Vol. 180, Part 1, No. 5, pp. 371-386, 1965-1966.
- [2] Dieudonne, J.E. et al, "An Actuator Extension Transformation for a Motion Simulator and an Inverse Transformation Applying Newton-Raphson's Method," *NASA Technical Report D-7067*, 1972.
- [3] Hoffman, R., and McKinnon, M.C., "Vibration Modes of an Aircraft Simulator Motion System," *Proc. The Fifth World Congress for the Theory of Machines and Mechanisms, an ASME Publication*, pp. 603-606, 1979.
- [4] McCallion, H., and Truong, P.D., "The Analysis of a Six-Degree-of-Freedom Work Station for Mechanised Assembly," *Proc. The Fifth World Congress for the Theory of Machines and Mechanisms, an ASME Publication*, pp. 611-616, 1979.
- [5] Hunt, K. H., *Kinematic Geometry of Mechanisms*, Oxford University, London 1978.
- [6] Sugimoto, K. and Duffy, J., "Application of Linear Algebra to Screw Systems," *Mech. Mach. Theory*, Vol. 17, No. 1, pp. 73-83, 1982.
- [7] Hunt, K. H., "Structural Kinematics of in-parallel-actuated Robot Arms," *Trans. ASME, J. Mech., Transmis., Automa. in Des.*, Vol. 105, pp. 705-712, 1983.
- [8] Premack, Timothy et al, "Design and Implementation of a Compliant Robot with Force Feedback and Strategy Planning Software," *NASA Technical Memorandum 86111*, 1984.
- [9] Nguyen, C.C., Pooran, F.J., and Premack, T., "Control of Robot Manipulator Compliance," in *Recent Trends in Robotics: Modeling, Control and Education*, edited by M. Jamshidi, J.Y.S. Luh, and M. Shahinpoor, North Holland, New York, pp. 237-242, 1986.
- [10] Yang, D. C. and Lee, T. W., "Feasibility Study of a Platform Type of Robotic Manipulators from a Kinematic Viewpoint," *Trans. ASME Journal of Mechanisms, Transmissions, and Automation in Design*, Vol. 106. pp. 191-198, June 1984.
- [11] Mohammed, M. G. and Duffy, J., "A Direct Determination of the Instantaneous Kinematics of Fully Parallel Robotic Manipulators," *ASME Journal of Mechanisms, Transmissions, and Automation in Design*, Vol. 107 pp. 226-229, 1985.
- [12] Fichter, E.F., "A Stewart Platform-Based Manipulator: General Theory and Practical Construction," *Int. Journal of Robotics Research*, pp. 157-182, Summer 1986
- [13] Sugimoto, K., "Kinematic and Dynamic Analysis of Parallel Manipulators by Means of Motor Algebra," *ASME Journal of Mechanisms, Transmissions, and Automation in Design*, pp. 1-5, Dec. 1986.
- [14] Lee, K. M., Chao, A., and Shah, D. K., "A Three Degrees of Freedom In-parallel Actuated Manipulator," *Proc. IASTED Int. Conf.*, pp. 134-138, 1986.
- [15] Rees-Jones, J., "Cross Coordinate Control of Robotic Manipulators," in *Proceedings of the International Workshop on Nuclear Robotic Technologies and Applications, Present and Future*, University of Lancaster, UK, June 29-July 1, 1987.
- [16] Behi, F., "Kinematic Analysis for a Six-Degree-of-Freedom 3-PRPS Parallel Mechanism," *IEEE Journal of Robotics and Automation*, Vol. 5, No. 5, pp. 561-565, October 1988.

- [17] Sharon, A., Hogan, N., Hardt, D., "High-Bandwidth Force Regulation and Inertia Reduction Using a Macro/Micro Manipulator System," *Proc. IEEE International Conference on Robotics and Automation*, pp. 261-266, Philadelphia, PA, April 1988.
- [18] Sugimoto, K., "Computational Scheme for Dynamic Analysis of Parallel Manipulators," in *Trends and Developments in Mechanisms, Machines, and Robotics-1988, ASME Proceedings of the 20th Biennial Mechanisms Conference*, 1988.
- [19] Kerr, D. R., "Analysis, Properties, and Design of a Stewart-Platform Transducer," in *Trends and Developments in Mechanisms, Machines, and Robotics-1988, ASME Proceedings of the 20th Biennial Mechanisms Conference*, 1988.
- [20] Nguyen, C.C., Pooran, F.J., "Adaptive Force/Position Control of Robot Manipulators with Closed-Kinematic Chain Mechanism," in *Robotics and Manufacturing: Recent Trends in Research, Education, and Application*, edited by M. Jamshidi et al, ASME Press, New York, pp. 177-186, 1988.
- [21] Griffis, M., Duffy, J., "A Forward Displacement Analysis of a Class of Stewart Platforms," *Journal of Robotic Systems*, Vol. 6, pp. 703-720, 1989.
- [22] Nguyen, C.C., and Pooran, F.J., "Kinematic Analysis and Workspace Determination of A 6 DOF CKCM Robot End-Effector," *Journal of Mechanical Working Technology*, Vol. 20, pp. 283-294, 1989.
- [23] Nguyen, C.C., and Pooran, F.J., "Dynamical Analysis of 6 DOF CKCM Robot End-Effector for Dual-Arm Telerobot Systems," *Journal of Robotics and Autonomous Systems*, Vol. 5, pp. 377-394, 1989.
- [24] Nanua, P., Waldron, K.J., Murthy, V., "Direct Kinematic Solution of a Stewart Platform," *IEEE Trans. Robotics and Automation*, Vol. 6, No. 4, pp. 438-444, 1990.
- [25] Nguyen, C.C., and Pooran, F.J., "Learning-Based Control of a Closed-Kinematic Chain Robot End-Effector Performing Repetitive Tasks," *International Journal of Microcomputer Applications*, Vol. 9, No. 1, pp. 9-15, 1990.
- [26] Nguyen, C.C., Antrazi, S., Zhou, Z-L, "Trajectory Planning and Kinematic Control of a Stewart Platform-Based Manipulator," *Proc. 5th International Conference on CAD/CAM Robotics and Factories of the Future*, pp. 493-499, Norfolk, Virginia, December 1990.
- [27] Nguyen, C.C., Antrazi, S., Zhou, Z-L, Campbell, Jr., C.E., "Experimental Study of Motion Control and Trajectory Planning for a Stewart Platform Robot Manipulator," *Proc. IEEE International Conference on Robotics and Automation*, pp. 1873-1878, Sacramento, California, April 1991.
- [28] Goodman, L.E. and Warner, W.H., "Statics," *Wadsworth Publishing Company, Inc.*, Belmont, California, 1963.
- [29] Press, W.H., et al, "Numerical Recipes in C: The Art of Scientific Computing," *Cambridge University Press*, 1988.
- [30] Fu, K.S. et.al., *Robotics: Control, Sensing, Vision, and Intelligence*, McGraw-Hill, New York, 1987.

CAMAC Data Acquisition System

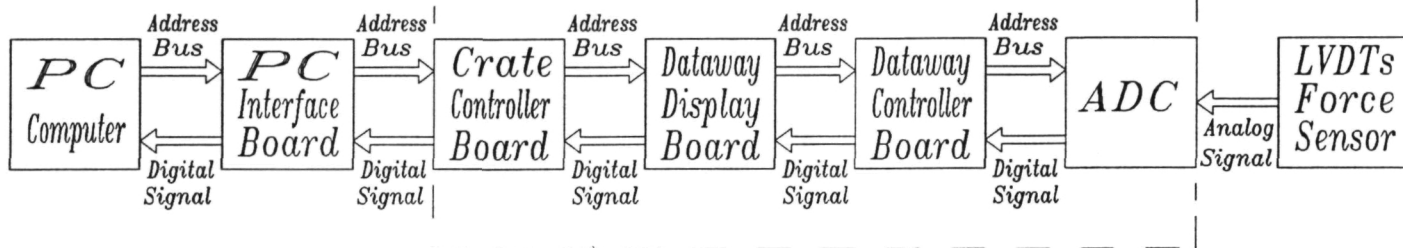


Figure 1: The force/torque sensor system

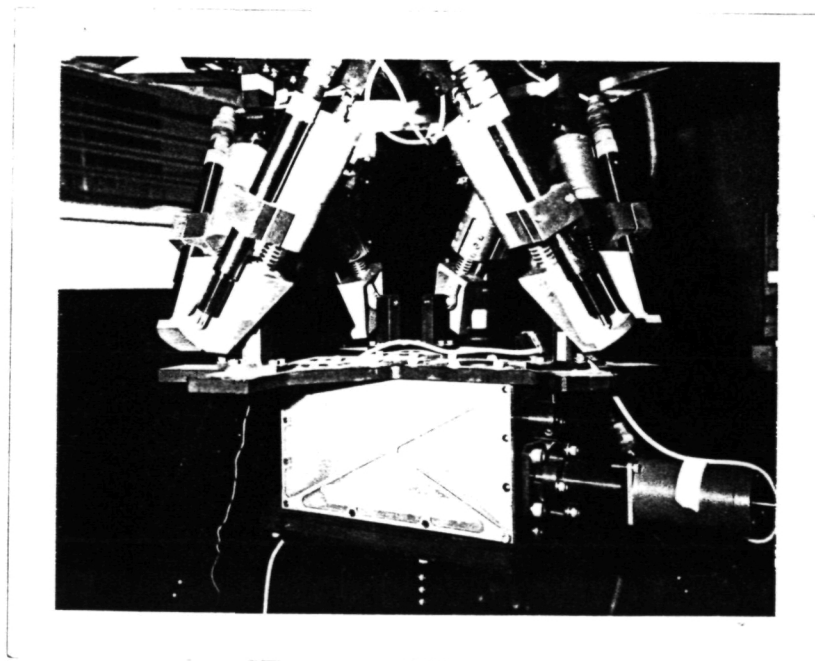


Figure 2: The Stewart Platform-based force/torque sensor

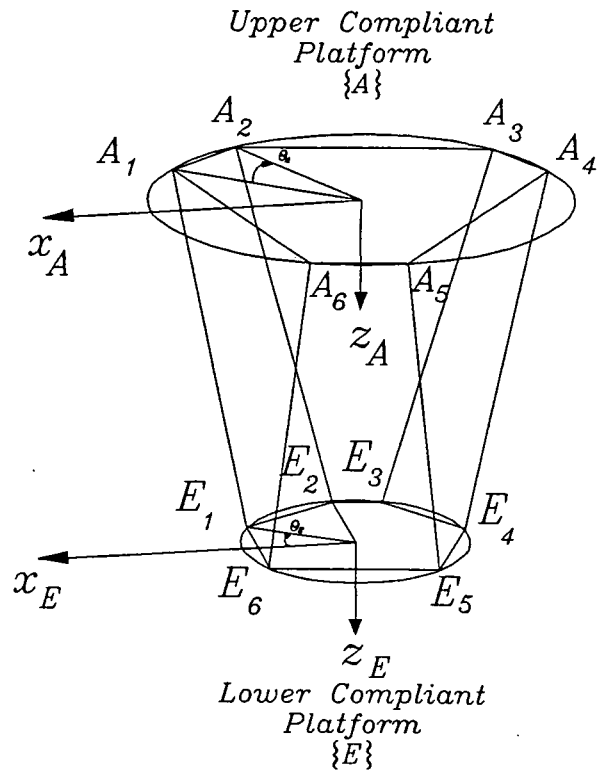


Figure 3: Frame assignment for the force/torque sensor

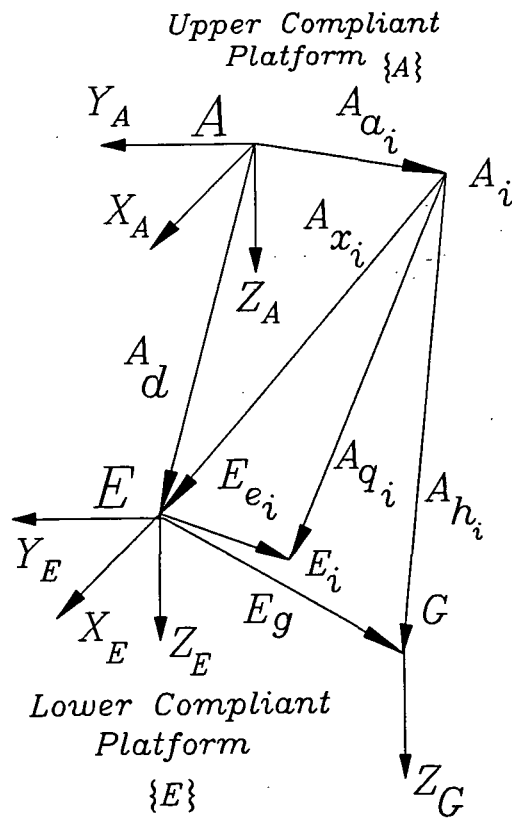


Figure 4: Vector diagram of the i th piston

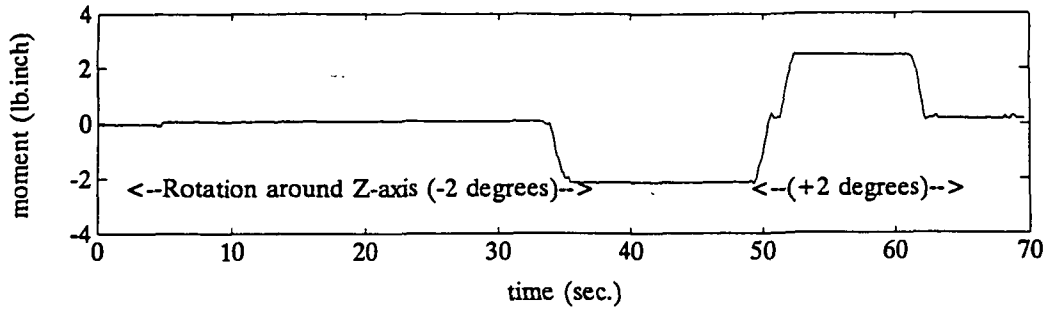


Figure 5: Torque about the z_G axis

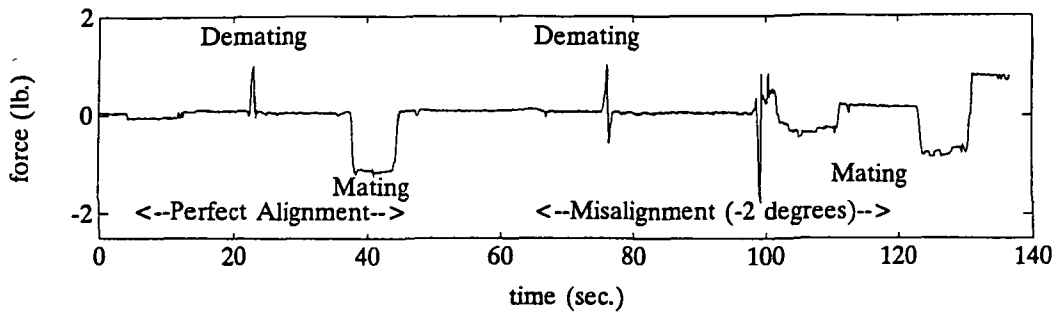


Figure 6: Force about the x_A axis

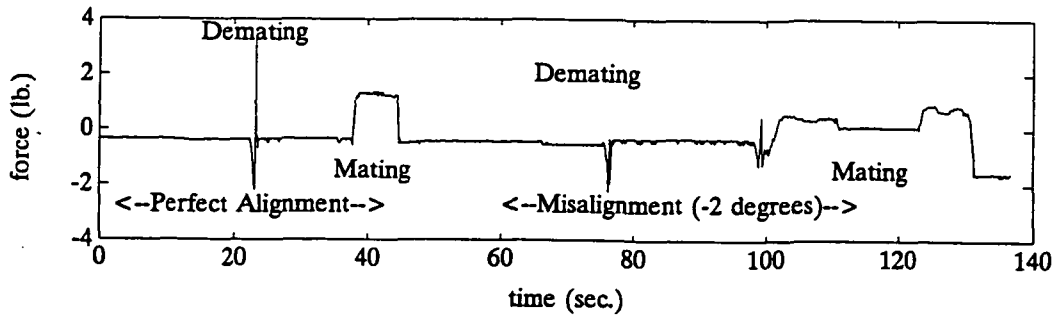


Figure 7: Force along the y_A axis

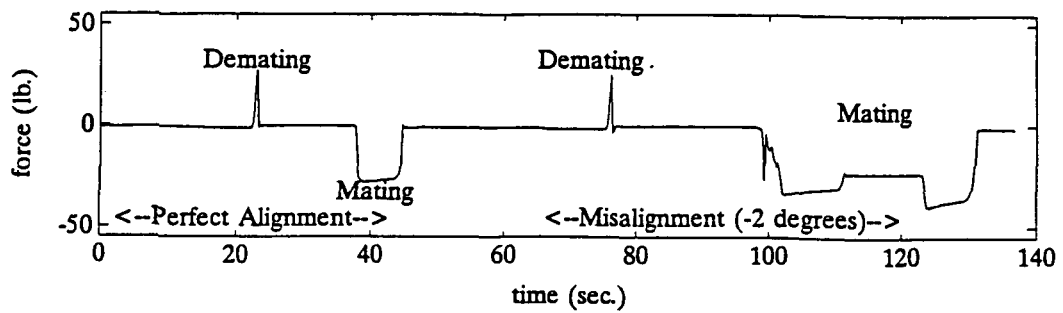


Figure 8: Force along the z_A axis

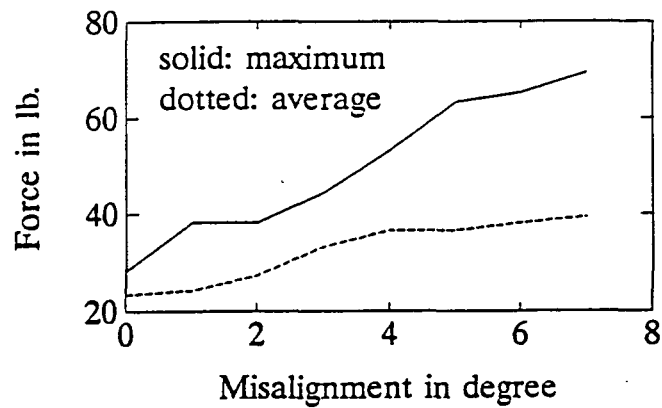


Figure 9: Mating forces versus misalignment degrees